

UNMANNED AERIAL VEHICLES

MEEC/MEAER

Lab 2 Report

Authors:

André Lopes Rodrigues (96576)
Keila Gomes Sanches (91151)
Daniel Fernando Brigham Évora (99473)
João André Tomé Lehodey (96538)

andre.rodrigues.01@tecnico.ulisboa.pt
keilasanches@tecnico.ulisboa.pt
dbrighamevora@tecnico.ulisboa.pt
joao.lehodey@tecnico.ulisboa.pt

Group 8

2023/2024 – 1st Semester

1 Q3 - Modelling and characterization of the sensors

In this section, experiments were done in order to model the sensors and characterize their noise and disturbances. With the data registered from each experiment, the mean value and the covariance matrix were obtained. The measurements, mean and covariance corresponding to each experiment are presented in dedicated subsections.

1.1 Experiment A

In Experiment A the quadrotor was kept stationary with its actuators turned off, such as to not let any noise originating from the motors interfere with the measurements being taken.

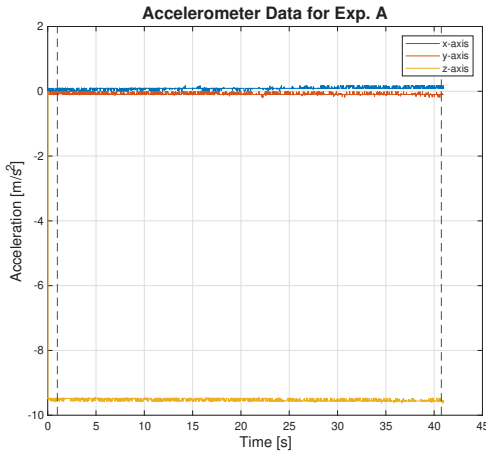


Figure 1: Accelerometer Data of Exp. A.

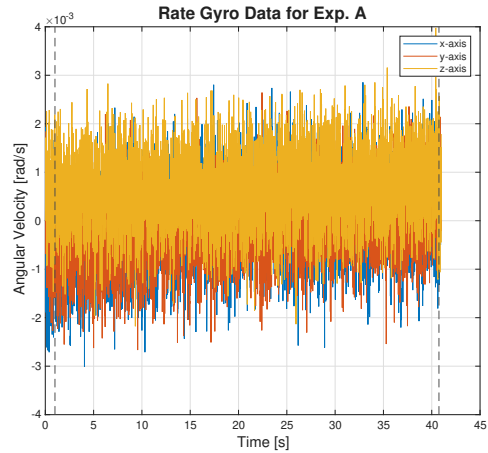


Figure 2: Rate Gyro Data for Exp. A.

The data in-between the black dashed lines (from $t = 1\text{ s}$ until the end) was used to compute the mean and covariance matrices.

For the accelerometer, the mean values obtained are 0.0896 m/s^2 in the x-axis, -0.0779 m/s^2 in the y-axis, and -9.5263 m/s^2 in the z-axis.

$$\text{The covariance matrix obtained for the accelerometer is } \begin{bmatrix} 14.2746 & -2.1235 & -3.0379 \\ -2.1235 & 11.2651 & 2.6336 \\ -3.0379 & 2.6336 & 13.4653 \end{bmatrix} \times 10^{-4} [\text{m}^2/\text{s}^4].$$

For the rate gyros, the mean values obtained are $7.6486 \times 10^{-6} \text{ rad/s}$ for the x-axis, $-1.1553 \times 10^{-4} \text{ rad/s}$ for the y-axis, and $6.5445 \times 10^{-4} \text{ rad/s}$ for the z-axis.

$$\text{The covariance matrix obtained for the rate gyros is } \begin{bmatrix} 0.6259 & 0.0522 & 0.0134 \\ 0.0522 & 0.5131 & 0.0245 \\ 0.0134 & 0.0245 & 0.5123 \end{bmatrix} \times 10^{-6} [\text{rad}^2/\text{s}^2].$$

In reality, these results, though expected, are different from the desired. The desired mean values for the accelerometers were 0 m/s^2 for the x- and y-axis, and $\approx 9.81 \text{ m/s}^2$ for the z-axis. These errors are likely due to an inherent bias in the sensors, either related to an imperfect placement/alignment of the sensor unit or to its intrinsic characteristics. Another possible causation is the fact that our quadrotor had a damaged support. The rate gyros mean values are closer to the expected 0 rad/s , which is in accordance with the drone being at rest.

Regarding the accelerometer and rate gyros covariance matrices, it's evident that the diagonal elements are larger than the off-diagonal elements, meaning that each axis measurement is relatively independent and there's likely minimal correlation between the different axis of each sensor.

1.2 Experiment B

In Experiment B the quadrotor was kept on the ground with its motors spinning by applying pressure on the hull to keep it from taking off. This was achieved by placing a hand on top of the hull.

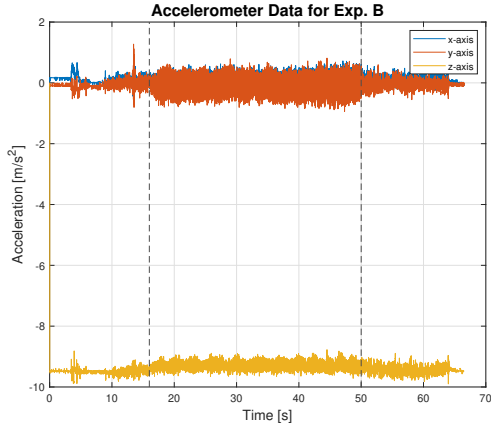


Figure 3: Accelerometer Data for Exp. B.

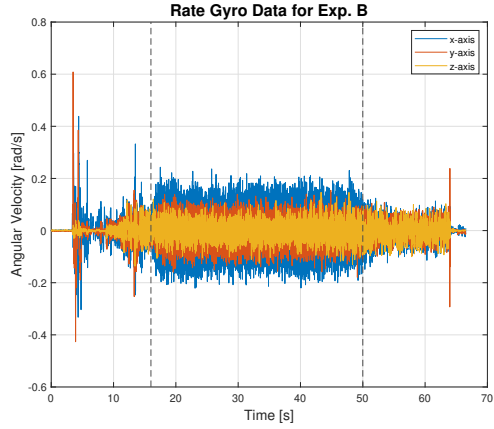


Figure 4: Rate Gyro Data for Exp. B.

The data in-between the black dashed lines (from $t = 16$ s to $t = 50$ s) was used to compute the mean and covariance matrices.

For the accelerometer, the mean values obtained are 0.0725 m/s^2 in the x-axis, -0.0964 m/s^2 in the y-axis, and -9.2861 m/s^2 in the z-axis.

$$\text{The covariance matrix obtained for the accelerometer is } \begin{bmatrix} 0.0463 & 0.0073 & -0.0139 \\ 0.0073 & 0.1054 & 0.0129 \\ -0.0139 & 0.0129 & 0.0162 \end{bmatrix} [\text{m}^2/\text{s}^4].$$

For the rate gyros, the mean values obtained are $-1.8742 \times 10^{-4} \text{ rad/s}$ for the x-axis, $-2.8540 \times 10^{-4} \text{ rad/s}$ for the y-axis, and $2.4691 \times 10^{-3} \text{ rad/s}$ for the z-axis.

$$\text{The covariance matrix obtained for the rate gyros is } \begin{bmatrix} 85.5606 & -35.6570 & -2.0689 \\ -35.6570 & 28.8095 & 4.9887 \\ -2.0689 & 4.9887 & 10.6467 \end{bmatrix} \times 10^{-4} [\text{rad}^2/\text{s}^2].$$

In Experiment B, the accelerometer mean values are slightly different when compared to [Experiment A](#) for the x- and y-axis, while the z-axis mean value sees a more significant deviation. This could be due to an improper experimental setup as it seems that there is a slight change in the average value in each axis of the accelerometer when the motor starts to spin, probably due to the way it was held down. This in turn, alters the orientation of the drone, leading to the acquisition of inaccurate measurements. Again, the higher overall mean values for the rate gyros can likely be attributed to the inappropriate manner in which the experiment was conducted (imbalanced application of the counteracting force might have led to slight movements of the drone). In comparison with [Experiment A](#), it's noticeable that the measurement uncertainty has risen. This is due to the drone's vibrations induced by the operation of its motors. It's also distinguishable that the overall values of the measurements get more noisy around $t = 17$ s. This is probably a consequence of the height control system of the drone full throttling the motors, which in turn leads to bigger vibrations of the hull, and higher uncertainty.

1.3 Experiment C

In Experiment C the quadrotor was kept in hover at a height of 0.75 m and with constant orientation.

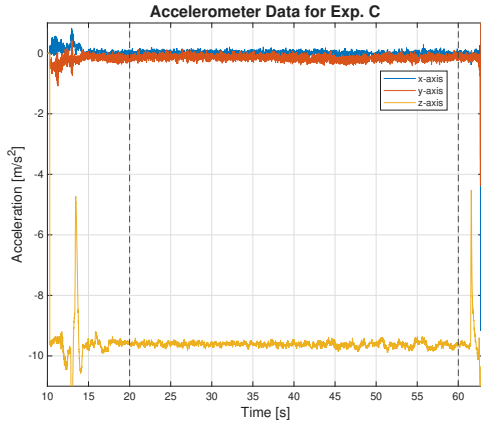


Figure 5: Accelerometer Data of Exp. C.

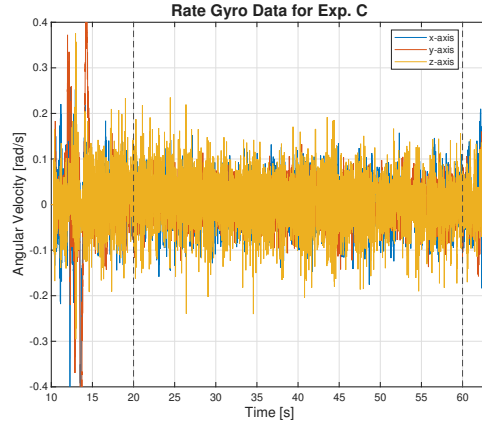


Figure 6: Rate Gyro Data for Exp. C.

The data in-between the black dashed lines (from $t = 20\text{ s}$ to $t = 60\text{ s}$) was used to compute the mean and covariance matrices.

For the accelerometer, the mean values obtained are -0.0108 m/s^2 in the x-axis, -0.1491 m/s^2 in the y-axis, and -9.6202 m/s^2 in the z-axis.

The covariance matrix obtained for the accelerometer is $\begin{bmatrix} 42.4108 & 3.6197 & 0.8320 \\ 3.6197 & 63.0022 & 7.4188 \\ 0.8320 & 7.4188 & 54.4877 \end{bmatrix} \times 10^{-4} [\text{m}^2/\text{s}^4]$.

For the rate gyros, the mean values obtained are $2.5232 \times 10^{-4}\text{ rad/s}$ for the x-axis, $-4.0830 \times 10^{-4}\text{ rad/s}$ for the y-axis, and $3.8450 \times 10^{-3}\text{ rad/s}$ for the z-axis.

The covariance matrix obtained for the rate gyros is $\begin{bmatrix} 19.9758 & -0.7554 & -4.0125 \\ -0.7554 & 11.6166 & -2.3283 \\ -4.0125 & -2.3283 & 25.3215 \end{bmatrix} \times 10^{-4} [\text{rad}^2/\text{s}^2]$.

The observed x- and y-axis accelerometer mean values are relatively different from the last experiments which is not unexpected since the hovering is never perfect and might result in some accelerations that are not properly corrected. To reduce these effects, we would need to acquire data for longer periods of time. However, the z-axis accelerometer mean value is as anticipated, taking a value closer to the ideal gravity and to the value obtained in [Experiment A](#). The rate gyros mean values keep up with expectations, staying close to zero. However, they show a slight increase in value when compared to [Experiment B](#). Specifically the z-axis mean shows the highest shift in absolute value. But these values are too small to take any meaningful conclusions.

While in [Experiment B](#), the main source of uncertainty is the vibration of the hull produced by the operation of the rotors, in Experiment C the sensors are affected not only by vibrations but also shifts in motor thrust to maintain the hover state, another source of larger deviations is the changes in accelerations to reach the desired height due to the height control. Regardless, Experiment C exhibits overall less uncertainty in comparison to [Experiment B](#). This might be an indication that vibration is the most significant source of noise for both the accelerometers and the rate gyros, which was greater in [Experiment B](#) due to the motors being operated at their maximum thrust. This also shows that hover control of the drone is quite good as the shifts in acceleration are small.

1.4 Raw Pitch and Roll Inclinometer Measurements

An estimate of the roll and pitch can be calculated from the accelerometer values. Assuming a stationary quadrotor, the value of the accelerometer is dominated by the acceleration of gravity. Using this information we can get that near hover condition:

$$\delta \propto -g [-\sin\theta \quad \cos\theta\sin\phi \quad \cos\theta\cos\phi]^T \quad (1)$$

from which we can derive the following equations for the roll and pitch:

$$\theta = \arcsin(\delta_x / ||\delta||_2); \quad \phi = \arctan(\delta_y / \delta_z) \quad (2)$$

Using the accelerometer data obtained from [Experiment C](#), the raw pitch and roll inclinometer measurements for each experiment were calculated where we noticed a bias in the inclinometer data. To solve this, the accelerometer mean values from [Experiment C](#) were subtracted from the accelerometer values used to compute the inclinometer data (not forgetting to take into consideration that the expected mean value for the z-axis accelerometer is $\approx 9.8 \text{ m/s}^2$). [Experiment C](#) was chosen due to the fact that the quadrotor used for this experiment had a damaged support and therefore the average value from [Experiment A](#) might not give us the correct bias. The obtained bias-free inclinometer data is shown below. From now on, the inclinometer will always be used with the removal of this bias.

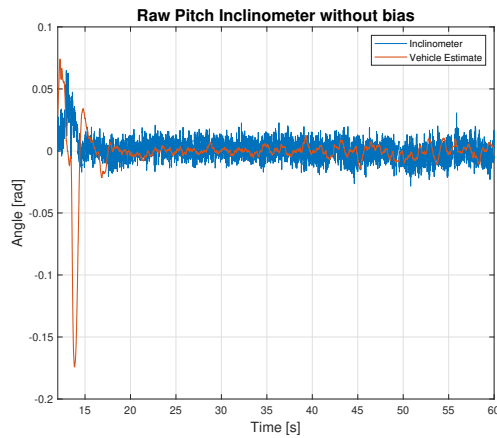


Figure 7: Pitch from Inclinometer without bias for Exp. C.

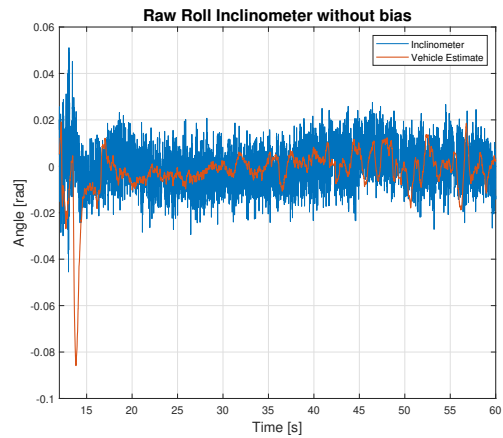


Figure 8: Roll from Inclinometer without bias for Exp. C.

From the plots above, the data between $t = 20 \text{ s}$ and $t = 60 \text{ s}$ was used to compute the variances of the inclinometer: $0.4418 \times 10^{-4} \text{ rad}^2$ for the pitch, and $0.6555 \times 10^{-4} \text{ rad}^2$ for the roll. It is noticeable that when hovering starts ($t = 17$), the estimate of the drone and inclinometer data are in sync. However the inclinometer is noisier, which is expected as we believe that the vehicle estimate uses a Kalman filter. We can also note that during takeoff, the vehicle estimate and inclinometer data have a larger discrepancy. This is due to the existence of accelerations caused by the rotors which we assume do not exist when designing the inclinometer.

2 Q4 - Kalman Filters

In this Section, we design and implement a state observer firstly for the pitch and lastly for the roll. For linear time-invariant systems (LTI) in continuous time, the equation that defines our state observer takes the form:

$$\dot{\hat{x}}(t) = \underbrace{A\hat{x}(t) + Bu(t)}_{P1} + \underbrace{L(y(t) - C\hat{x}(t))}_{P2} \quad (3)$$

where \hat{x} is our state estimate. We can see that the first part ($P1$) of the equation corresponds to a replica of our system. The second part ($P2$) will ensure that our estimate converges to the real value of the state.

We may quickly look at the error equation to understand what is happening. Defining $\tilde{x} = x - \hat{x}$,

and getting the differential equation that describes the error, we get:

$$\begin{aligned}\dot{\hat{x}} &= \dot{x} - \hat{x} \\ \dot{\hat{x}} &= A(x - \hat{x}) - LC(x - \hat{x}) \\ \dot{\tilde{x}} &= (A - LC)\tilde{x}\end{aligned}$$

It is now obvious that for the estimation error to converge to 0, we need the matrix $(A - LC)$ to have eigenvalues with negative real part.

The vector of gains L is chosen by us. A possible way of designing the controller is by choosing the vector of gains L as to place the poles of $(A - LC)$ in a predefined place which is always possible given that the pair (A, C) is observable. One may think that placing the eigenvalues as close as possible to negative infinity would be ideal since the convergence time would tend to zero, this would be true in a perfect world, however, this is not true since both our model and measurements have noise. Instead, we will use the Kalman gain. Given an observable LTI system defined as:

$$\begin{aligned}\dot{x}(t) &= Ax(t) + Bu(t) + w \\ y(t) &= Cx(t) + n\end{aligned}$$

where w and n denote the model noise and the measurement noise respectively. These are assumed to follow a normal distribution of covariances Q and R , respectively, with zero mean and are independent. The Kalman Gain L_k is such that:

- It minimizes $\int_0^{\inf} ||\tilde{x}(t)||^2$;
- Estimation error is centered, $E[\tilde{x}(t)] = 0$;

and is given by:

$$L_k = \Sigma C^T R \quad (4)$$

where Σ is the only positive definite solution of the Riccati Algebraic Equation given by:

$$A\Sigma + \Sigma A^T + Q - \Sigma C^T R^{-1} C \Sigma = 0; \quad (5)$$

2.1 Pitch Estimation

In this Section we implemented a Kalman filter to estimate the pitch of the vehicle. The model used corresponds to a first order LTI model,

$$\begin{aligned}\dot{\theta} &= q \\ y &= \theta\end{aligned} \quad (6)$$

which is an approximation of the evolution of the pitch angle when close to a hover state, where the pitch and roll angles are small. The state variable θ corresponds to the pitch angle and q is its angular rate. In this case the evolution of $\hat{\theta}$ is described by Equation 3 with $A = 0$, $B = 1$, $C = 1$.

2.1.1 Estimation without considering the gyro bias

We will assume that the rate gyro measurement is $\omega_{ym} = q$, and that this measurement has noise w_θ , with variance Q , and that the inclinometer pitch measurement is $\theta_m = \theta$, which has noise n_θ , with variance R . From the model (6), we get

$$\dot{\theta} = \omega_{ym} + w_\theta \quad (7)$$

$$y = \theta_m + n_\theta \quad (8)$$

Later we will add a bias term due to gyro drift. However considering our current model, and since we characterized the gyro noise in Section 1 we can use the identified variance to design our Kalman filter. Similarly, in the same Section, we characterized the inclinometer measurement model noise which in this case corresponds to n_θ . The value of Q might still need some tuning since our model is only an approximation. The simulation results can be seen below where the above linear system was simulated and an observer was used. White noise was added to both the measurement and the model with variances 0.2 rad^2 and $0.2 \text{ rad}^2/\text{s}^2$, therefore $R = Q = 0.2$ when calculating the Kalman gains. We can see that even though the initial estimate is different than the state, over time it will approximate the state.

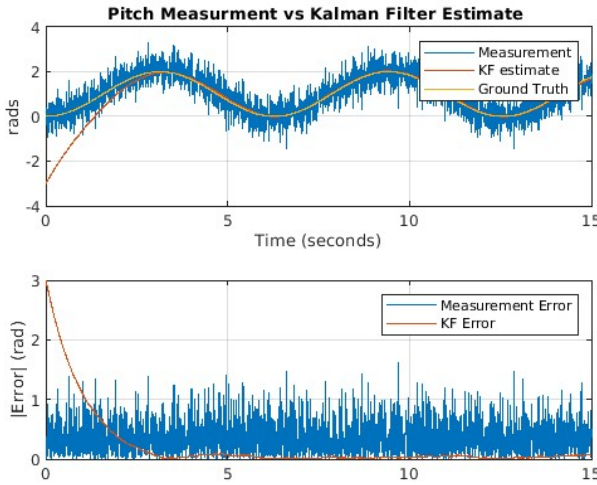


Figure 9: Simulation of our linear system with added noise, and sin wave input.

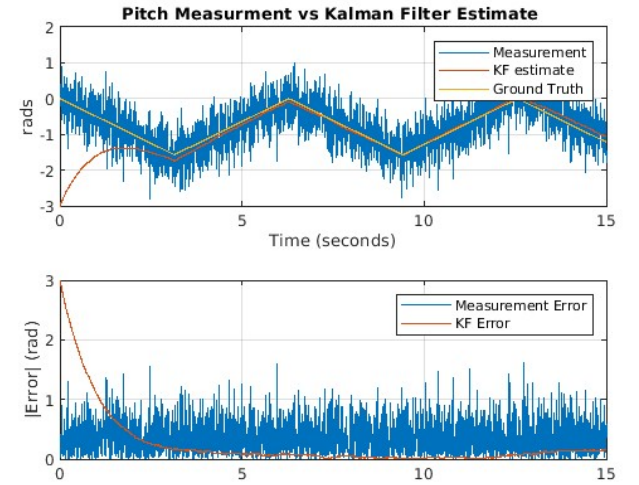


Figure 10: Simulation of our linear system with added noise, and square wave input.

It is also clear that the estimate of the state given by the Kalman filter has a much smaller average error after the initial convergence over the measured state error. Experimental results are provided in Subsection 2.1.6.

2.1.2 Transfer Function

From the model (6), the state estimate equation (3), and the previous definitions for the measurements, we obtain the transfer functions between the pitch inclinometer measurement and the pitch estimate, and the pitch rate gyro measurement and the pitch estimate. For the first, we assume that $\omega_{ym} = 0$,

$$\dot{\hat{\theta}} = L_k(\theta_m - \hat{\theta}) \xrightarrow{\mathcal{L}} \frac{\hat{\theta}(s)}{\theta_m(s)} = \frac{L_k}{s + L_k} \quad (9)$$

For the second transfer function, assuming $\theta_m = 0$, we get

$$\dot{\hat{\theta}} = \omega_{ym} + L_k(0 - \hat{\theta}) \xrightarrow{\mathcal{L}} \frac{\hat{\theta}(s)}{\omega_{ym}(s)} = \frac{1}{s + L_k} \quad (10)$$

Both transfer functions exhibit low-pass filter characteristics, sharing a common cutoff frequency (L_k). The distinguishing factor lies in their respective gains: one possesses a unitary gain, while the other is characterized by a gain of $\frac{1}{L_k}$.

2.1.3 Impact of parameters Q and R

Parameters Q and R correspond to the covariances of the model's noise and measurement noise, respectively. In real applications these are often used as "tuning knobs" since the covariances may be

hard to measure, especially the one from the model. These parameters can be thought off as how much "trust" is given to the model compared to the measurement. If Q is much larger than R , the filter will apply large corrections given the measurement, since it is more likely that the measurement is closer to the real state. However if R is much larger than Q , then the measurements are very noisy and more importance will be given to the estimate produced by our model, the measurements will provide smaller corrections.

For our system, using $R = 0.01$ and $Q = 0.1$ yields a Kalman gain of 3.16 which is much larger than if using $R = 0.1$ and $Q = 0.01$ which yields a Kalman gain of 0.316, as expected. It is also important to note that in the case where R and Q are scalars only the ratio between the Q and R matters.

2.1.4 Inclusion of the bias

To account for the bias term in the rate gyro, the model (6) is augmented with a new state, that corresponds to the bias. Assuming the bias is constant, we may model its dynamics, and also the modified rate gyro measurement, respectively as:

$$\dot{b}_y = 0; \quad \omega_{ym} = q + b_y \quad (11)$$

The resulting state-space model is expressed as:

$$\underbrace{\begin{bmatrix} \dot{\theta} \\ \dot{b}_y \end{bmatrix}}_{\dot{x}} = \underbrace{\begin{bmatrix} 0 & -1 \\ 0 & 0 \end{bmatrix}}_A \underbrace{\begin{bmatrix} \theta \\ b_y \end{bmatrix}}_x + \underbrace{\begin{bmatrix} 1 \\ 0 \end{bmatrix}}_B \underbrace{\omega_{ym}}_u \quad (12)$$

$$\underbrace{\begin{bmatrix} \theta \\ y \end{bmatrix}}_x = \underbrace{\begin{bmatrix} 1 & 0 \end{bmatrix}}_C x \quad (13)$$

This system is observable since the observability matrix $\mathcal{O}(C, A)$ is full column rank, meaning we can design a state observer.

The simulation results, shown in the following figures, demonstrate the performance of the Kalman filter (Equation 3) in estimating the state variables. Gaussian additive noise was added to the gyro measurement and to the pitch measurement with variances 0.2 rad^2 and $0.2 \text{ rad}^2/\text{s}^2$ respectively. Q was set to $I_{2 \times 2}$ and R to 1.

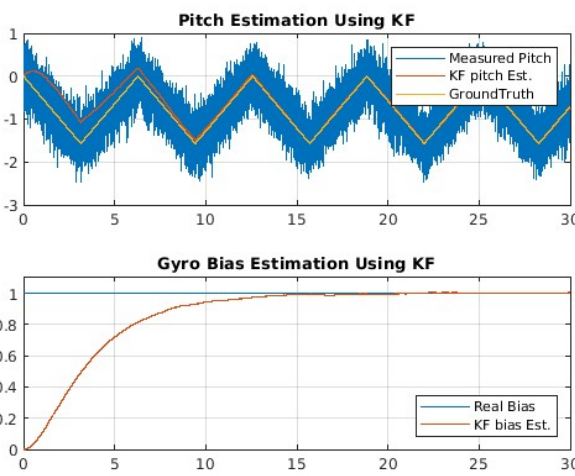


Figure 11: Simulation of our linear system with added noise, and gyro bias using square wave input.

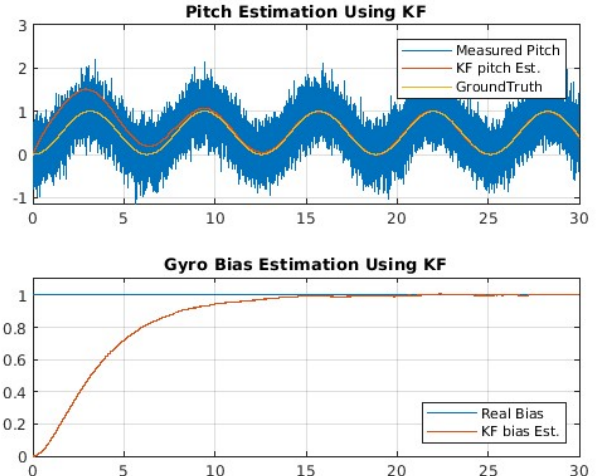


Figure 12: Simulation of our linear system with added noise, and gyro bias using sin wave input.

The Kalman filter provides accurate estimates for the state variables after the initial convergence, driving the error of both the bias and pitch estimate to zero as expected. Again, experimental results are provided in Subsection 2.1.6.

2.1.5 Complementarity of the filters

From the previously obtained transfer functions in Subsubsection 2.1.2, applying the superposition principle we have:

$$\hat{\theta}(s) = \frac{L_k}{s + L_k} \theta_m(s) + \frac{s}{s + L_k} \frac{\omega_{ym}(s)}{s} \quad (14)$$

We can express the individual transfer functions of the complementary filter as follows:

$$G_1(s) = \frac{L_k}{s + L_k}; \quad G_2(s) = \frac{s}{s + L_k} \quad (15)$$

and the sum of $G_1(s)$ and $G_2(s)$ yields:

$$G_1(s) + G_2(s) = \frac{L_k}{s + L_k} + \frac{s}{s + L_k} = 1 = 0dB \quad (16)$$

Regarding the Kalman filter implemented in the previous Subsubsection, we can verify that it is also a complementary filter. To do so, we use Equation (3) to obtain,

$$\dot{x}(t) = (A - L_k C) \hat{x}(t) + B \omega_{ym} + L_k \theta_m \quad (17)$$

where A , B , C are the same as in (12) and (13), and $L_k = [L_1, L_2]^T$ is the kalman gain. Using the superposition principle, and applying the Laplace Transform, we get,

$$G_{LP} = \frac{L_1 s + L_2}{s^2 + L_1 s + L_2}; \quad G_{HP} = \frac{s^2}{s^2 + L_1 s + L_2} \quad (18)$$

which verifies $G_{HP} = 1 - G_{LP}$, thus making it a complimentary filter.

The following bode magnitude plots illustrate the previous results:

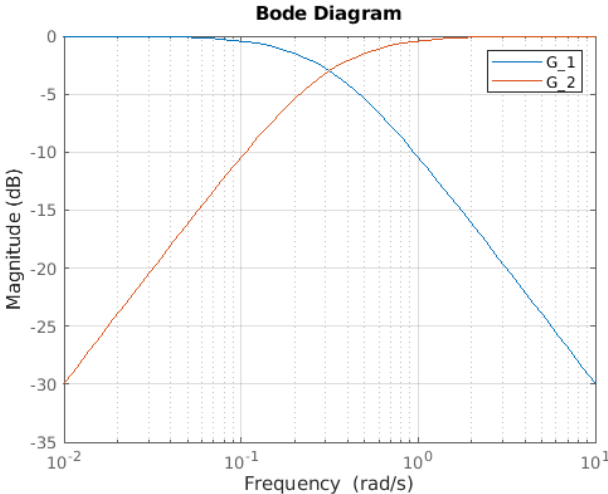


Figure 13: Bode Magnitude Plot of Transfer Functions (15) (simple KF), with $L_k = 0.316$.

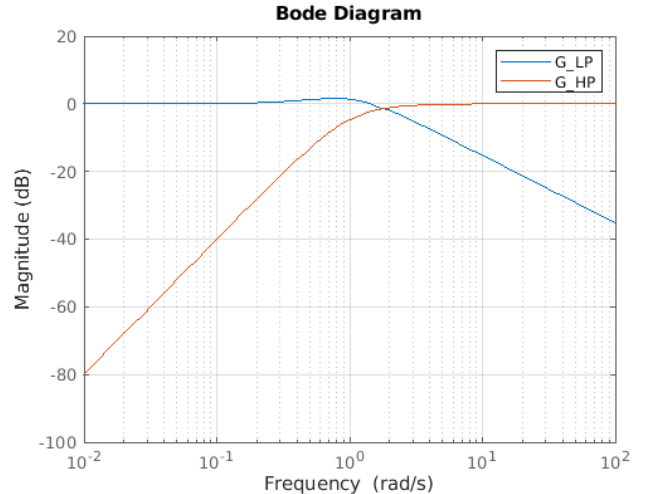


Figure 14: Bode Magnitude Plot of Transfer Functions (18) (augmented KF), with $L_k = [1.7, -1]^T$.

The presented graphic illustrates the synergy between the two filters employed. Specifically, at higher frequencies, the pitch estimation is predominantly influenced by the rate gyro measurement, while at lower frequencies, the inclinometer measurement assumes greater significance.

The complementary filter, prioritizes the most effective sensor within a specific frequency range. Its ease of implementation and minimal computational requirements make it advantageous. However, challenges arise from the integration of gyroscope noise, which can lead to error accumulation or drift over time. In real world application the noise is not really white, a potential mismatch between the predetermined filter parameters and actual noise levels measured by the sensor may impact its performance.

2.1.6 Experimental Results and Experiment Differences

In this Subsubsection we present the experimental results. Firstly, it's important to note that we lack access to the ground truth. Therefore, we compare the inclinometer results and the vehicle filter with our results as a sanity check. We also use various values of Q and R which allows us to compare their effect on the observed state. For the first Kalman filter, Q and R are scalars and therefore only their ratio is mentioned. The values labeled as original correspond to the $Q = \text{cov}(\omega_{ym})$ and $R = \text{cov}(\theta_m)$ obtained from Experiment C in Subsection 1.3.

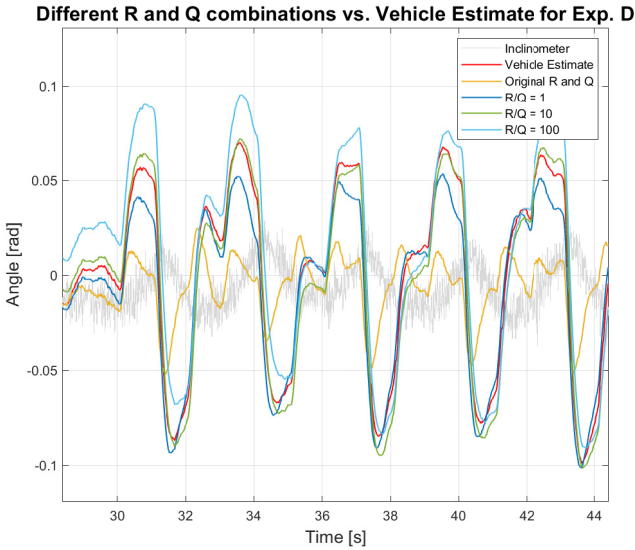


Figure 15: Pitch Kalman filter Exp. D, (simple KF).

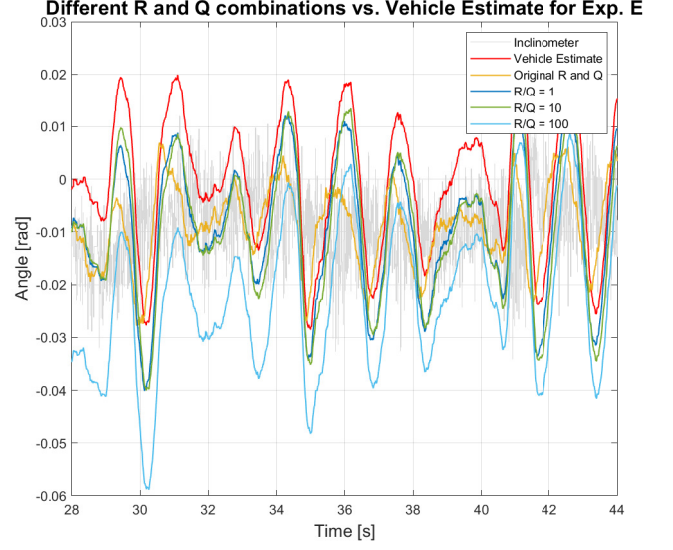


Figure 16: Pitch Kalman filter Exp. E, (simple KF).

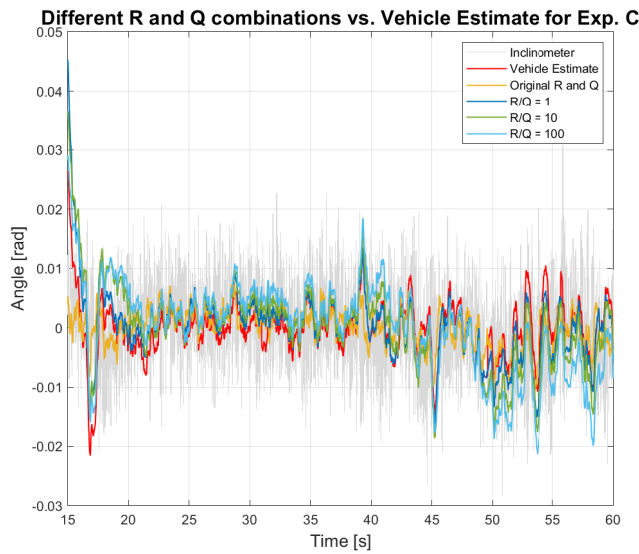


Figure 17: Pitch Kalman filter Exp. C, (simple KF).

Firstly we may notice from Figure 16 that there is an offset between the vehicle estimate and our estimate by approximately a constant value. This is a recurrent event during the experiments. These errors are due to different calibrations: the vehicle calibrates the accelerometer during start up which may be affected by the drone positioning especially due to the damaged support, while our inclinometer is calibrated using the values from Experiment C during hovering.

We notice that when R/Q is greater, more importance is given to the model. This results in larger displacements from the measured angles. Our estimate was closest to the one from the vehicle when

using $R/Q = 10$. It is also important to note that the inclinometer assumes no other accelerations than the one of gravity, therefore when the vehicle accelerated due to a pitch or roll angle, greater discrepancy between the estimate and the measurement is observed.

For the augmented model, we set $Q = \text{diag}([4.4 \times 10^{-5}, 10^{-12}])$ then R was changed as seen in the following graphs.

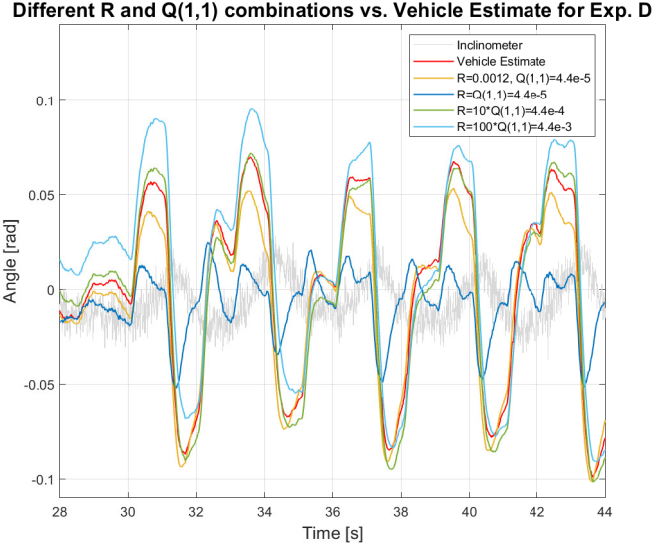


Figure 18: Pitch Augmented KF Exp. D.

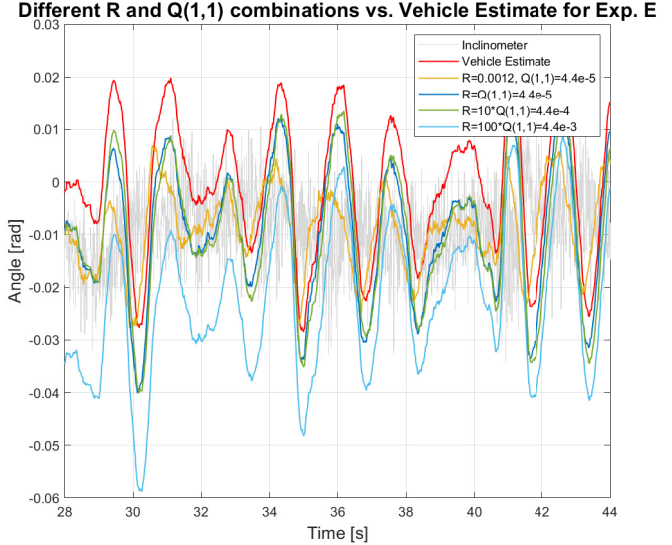


Figure 19: Pitch Augmented KF Exp. E.

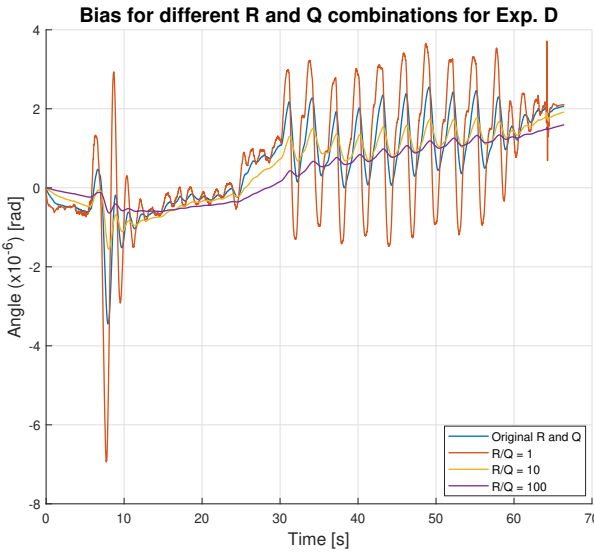


Figure 20: Rate Gyro Bias Augmented KF Exp. D.

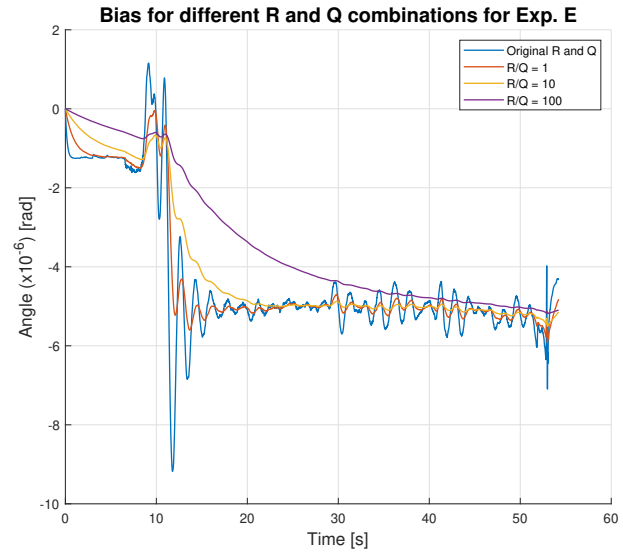


Figure 21: Rate Gyro Bias Augmented KF Exp. E.

For the augmented model, the observations for the pitch and roll are similar, again as we increase R , more trust is given to the model. Obviously, our model now also has a constant bias, therefore when more trust is given to the model, a slower change of the bias is seen, with far less oscillations as expected. We can however see that the bias estimates tend to the same value independently of its transitory behaviour. To reduce the number of degrees of freedom we kept Q constant. However we could have studied the effect of changing the model noise characteristics by experimenting with different Q matrices.

Finally, we can compare the results for the different experiments. For Experiment C, since the quadrotor is always in hover, the measurement model and the dynamics model are in sync since they

are both approximations close to hover, this translates to our pitch estimate resembling the output of a low pass filter of the measured inclinometer data as seen in Figure 17. In Experiments D and E, more discrepancy is seen between the measurements and the estimate especially when a larger R is employed, as expected.

2.2 Roll Estimation

In this Subsection, the same procedure as the one described in Subsection 2.1 was followed, but now with the intent of estimating the roll of the drone.

To do so, the following state-space model was used,

$$\begin{aligned}\dot{\phi} &= p \\ y &= \phi\end{aligned}\tag{19}$$

where the state variable ϕ corresponds to the roll angle and p is its angular rate. This is an approximation of the roll dynamics close to hover. One can clearly notice that the equations that describe the roll dynamics are similar to the ones that describe the pitch dynamics.

2.2.1 Estimation without considering the bias

Neglecting the presence of a bias in the measurements, the values obtained by the inclinometer and rate gyro are respectively, $\phi_m = \phi$ and $\omega_{xm} = p$. Using (19), we get

$$\dot{\phi} = \omega_{xm} + w_\phi\tag{20}$$

$$y = \phi_m + n_\phi\tag{21}$$

where w_ϕ and n_ϕ are the noises that characterize the rate gyro and inclinometer measurements, respectively.

The state-space equations derived for the roll, as expressed in equations 20 and 21, are evidently identical to those previously obtained for the pitch Kalman filter. Consequently, the simulation outcomes for roll estimation are expected to mirror those observed in the pitch simulation (refer to Figures 9 and 10). This assumption holds under the premise of employing equivalent noise and disturbance conditions as previously considered in the pitch simulation.

2.2.2 Transfer Functions

Since the Kalman filter implemented for the roll estimation has the same model and measurements, we get the transfer functions,

$$\frac{\hat{\phi}(s)}{\phi_m(s)} = \frac{L_k}{s + L_k}; \quad \frac{\hat{\phi}(s)}{\omega_{xm}(s)} = \frac{1}{s + L_k}\tag{22}$$

These have the same characteristics as described in Subsubsection 2.1.2.

2.2.3 Impact of parameters Q and R

Because the model used for the roll estimation is the same used for the pitch, the effects described in Subsubsection 2.1.3 also apply to this Kalman filter implementation.

2.2.4 Inclusion of the bias

Including the effect of the bias, b_x in the rate gyro measurement,

$$\omega_{xm} = p + b_x\tag{23}$$

and augmenting the state to include the bias, with $\dot{b}_x = 0$, we get

$$\underbrace{\begin{bmatrix} \dot{\phi} \\ \dot{b}_x \end{bmatrix}}_{\dot{x}} = \underbrace{\begin{bmatrix} 0 & -1 \\ 0 & 0 \end{bmatrix}}_A \underbrace{\begin{bmatrix} \phi \\ b_x \end{bmatrix}}_x + \underbrace{\begin{bmatrix} 1 \\ 0 \end{bmatrix}}_B \omega_{xm} \quad (24)$$

$$y = [1 \ 0] x \quad (25)$$

These again take the same form as the equations from Subsubsection 2.1.4.

2.2.5 Complementarity of the filters

Because the configuration of the Kalman filters implemented for roll estimation are the same as the ones for pitch estimation, we reach the same conclusions regarding the complementarity of the Kalman filters as those discussed in Subsubsection 2.1.5.

2.2.6 Experiment Differences

Here similar results to the ones obtained for the pitch were observed. Again, constant offsets between the vehicle estimate and the observed state estimate are present due to different calibration values.

As before we can clearly see that as R increases, the estimates are further away from the measurements as more importance is given to the model.

It is interesting to see that the Kalman filter for Experiment E is as expected. The experiment cycle starts at time $t \approx 28$ s where we have positive roll while the drone accelerates in the y direction, followed by a negative roll making the vehicle decelerate to a stop, followed by a plateau that corresponds to hover state. Then this procedure is repeated in the opposite order, thus returning the drone to its initial position.

As expected and as seen for pitch, when greater values of roll are reached, the estimate is further from the measurement as seen in Figure 23, due to the assumption that only the acceleration of gravity acts on the vehicle when calculating the roll and pitch from the accelerometer data. This is in contrast to 22 where measurements and estimates are in closer agreement.

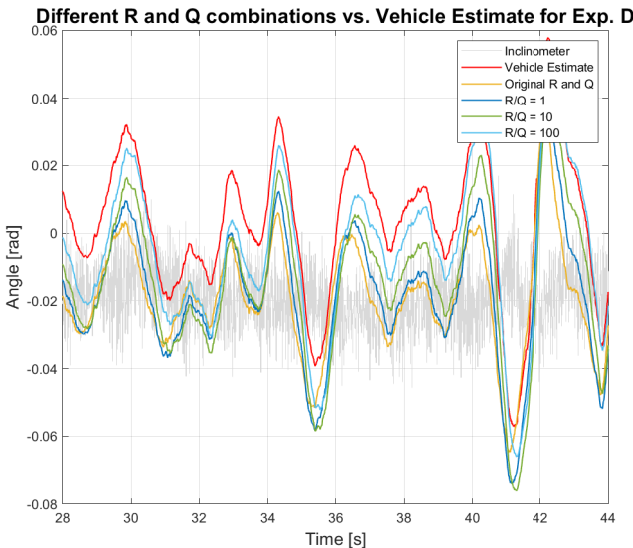


Figure 22: Roll KF Exp. D.

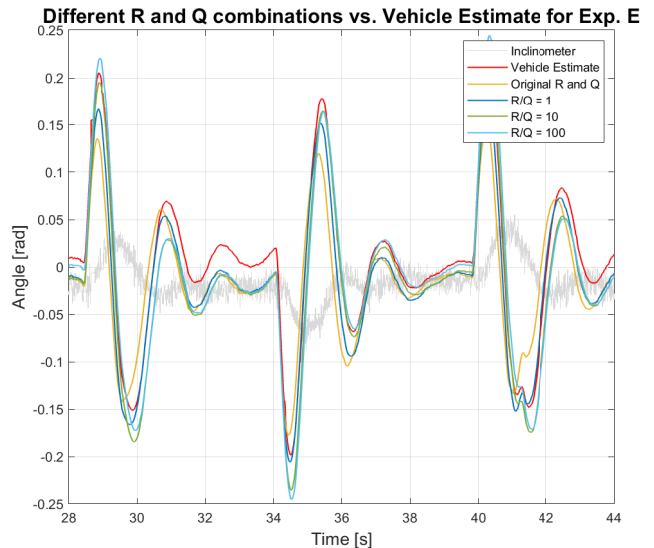


Figure 23: Roll KF Exp. E.

For the augmented model, we set $Q = \text{diag}([6.6 \times 10^{-6}, 10^{-12}])$ then R was changed as seen in the following graphs.

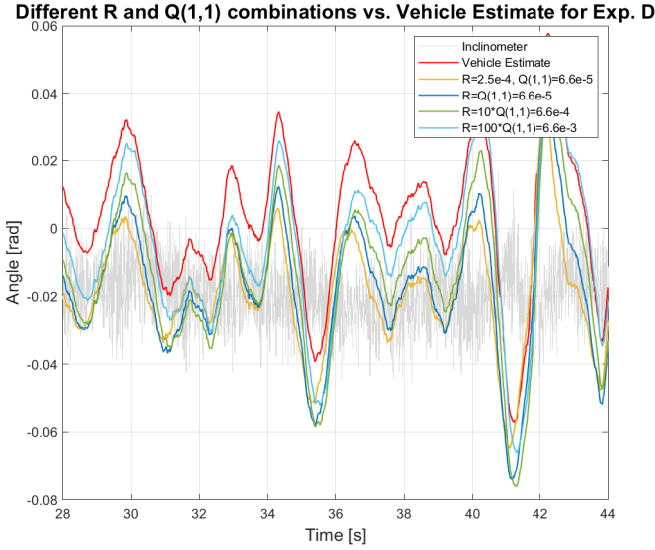


Figure 24: Roll Augmented KF Exp. D.

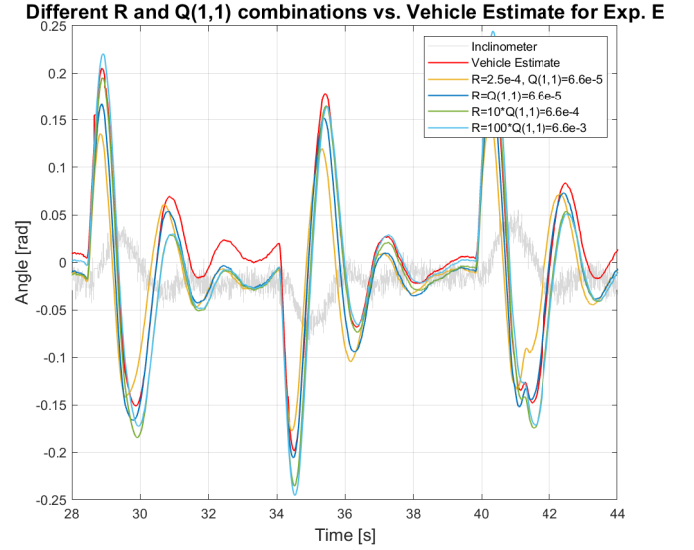


Figure 25: Roll Augmented KF Exp. E.

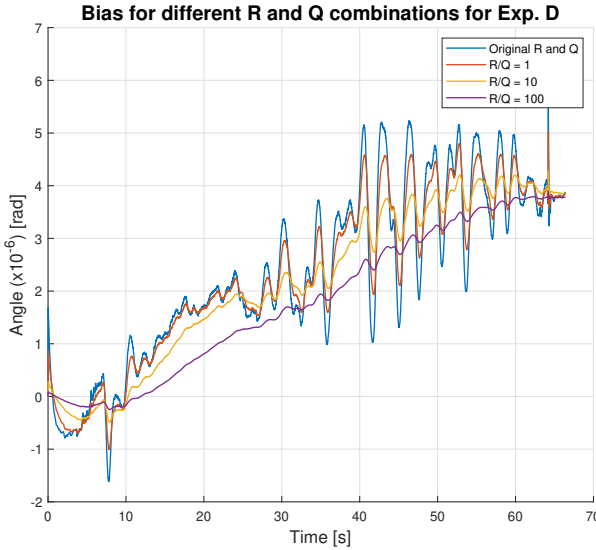


Figure 26: Rate Gyro Bias Augmented KF Exp. D.

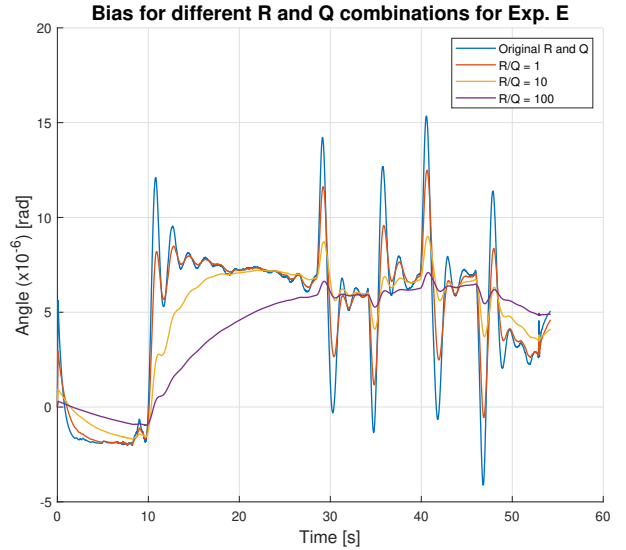


Figure 27: Rate Gyro Bias Augmented KF Exp. E.

Here the results are again concordant to the ones seen during the pitch experiments. The bias estimate shows greater oscillatory behaviour when smaller values of R are used, as less importance is given to the model in which the bias is set to constant. It is however still possible to see that even though the transitory regime is different, the bias estimate seems to be converging to the same value independently of the R ratios that were tested.

Next time, we should take measurements over larger periods of time, and acquire a ground truth to be able to properly compare all the obtained models.

3 Q5 - Integrated roll and pitch estimation

In this section we implement the filter proposed by Batista et al. (2011) [1]. We will assume that we have a known constant vector in inertial coordinates, and a measure of that vector in body coordinates. In this case we consider the accelerometer measurements which are dominated by gravity at low frequencies. Our state is then $x(t) \in \mathbb{R}^6 = [x_1, x_2]^T$ where x_1 is the gravity vector in body coordinates and x_2 corresponds to the bias of the gyro in each of its components.

Although the system is non-linear, since a sensor based approach is taken, the authors are able to reach a time varying system given that the measurement $y(t) = x_1(t)$ is available. The system becomes:

$$\dot{x}(t) = \begin{bmatrix} -S[\omega_m(t)] & -S[y(t)] \\ \mathbf{0}_{3 \times 3} & \mathbf{0}_{3 \times 3} \end{bmatrix} x(t) = A(y(t), \omega_m)x(t) \quad (26)$$

$$y(t) = [\mathbf{I}_{3 \times 3} \ \mathbf{0}_{3 \times 3}] x(t) = Cx(t) \quad (27)$$

for which a Kalman filter is implemented, therefore our observer equations are:

$$\dot{\hat{x}}(t) = A(y(t), \omega_m)\hat{x}(t) + L_k(t)(y(t) - C\hat{x}(t)) \quad (28)$$

with:

$$L_k(t) = P(t)C^T\Theta^{-1} \quad (29)$$

$$\dot{P}(t) = A(t)P(t) + P(t)A(t)^T + \Sigma + P(t)C^T\Theta^{-1}CP(t) \quad (30)$$

To test the algorithm, we simulated the system using additive zero mean white noise with variance $0.01 \text{ m}^2/\text{s}^4$ for the acceleration measurements and $0.01\pi/180 \text{ rad}^2/\text{s}^2$ for the angular velocity measurements. Setting the gyro bias to $[2, -3, 1]^T\pi/180 \text{ rad/s}$, $P(0) = 10I_{6 \times 6}$, the measurement model covariance $\Theta = 0.01I_{3 \times 3}$ and error model covariance $\Sigma = \text{diag}(0.05I_{3 \times 3}, 0.01I_{3 \times 3})$, where $\text{diag}(F, V)$ corresponds to the diagonal by blocks matrix with blocks F and V . The results obtained can be seen below.

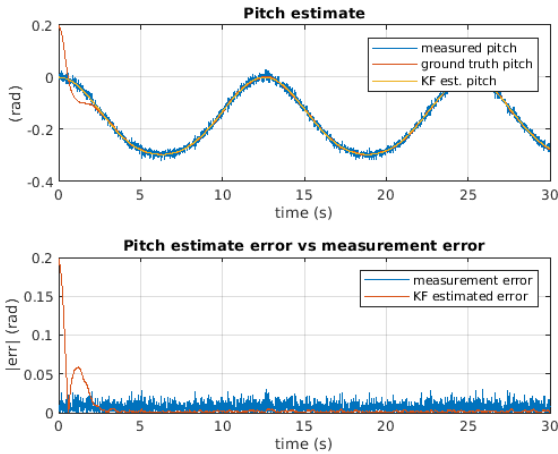


Figure 28: Pitch Estimate compared to measurement and ground truth.

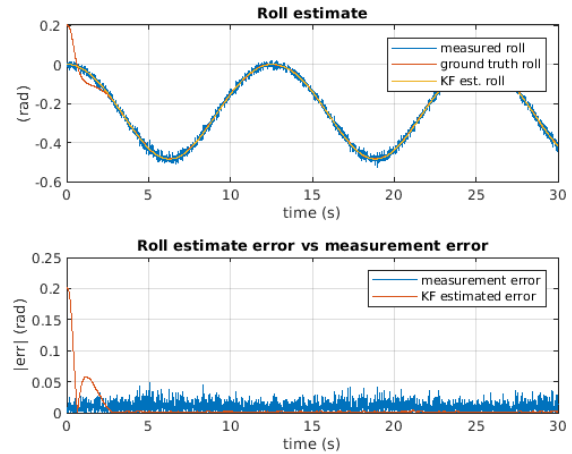


Figure 29: Roll Estimate compared to measurement and ground truth.

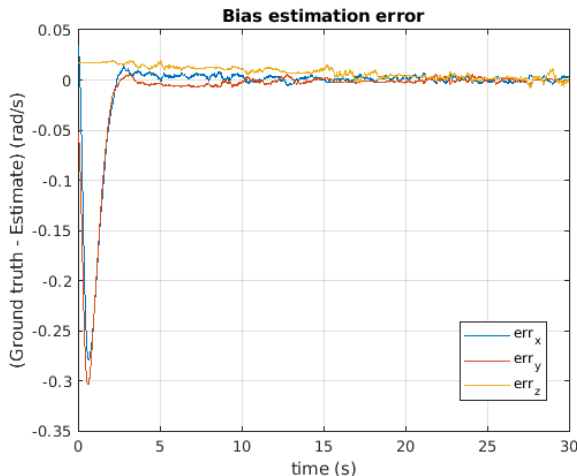


Figure 30: Error in bias estimate in each of the gyro components.

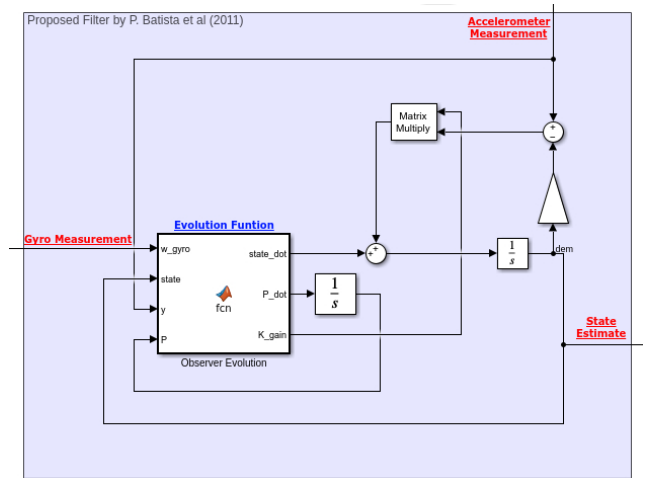


Figure 31: Simulink implementation of the proposed filter.

In the filter implementation 31, the evolution function calculates \dot{P} and L_k from Equations 30 and 29, it also calculates the first term of $\dot{\hat{x}}$ as seen in Equation 28, the second term is calculated using the Kalman gain and the error between the estimated measurement and the real measurement and is added later. We can see that even though the initial values are incorrect, the estimation error decreases rapidly and then stays close to 0 for both the pitch and the roll. From the estimation error versus the measurement error, the advantage of using this filter is evident since the measurement error has a larger expected absolute error after the initial convergence of the Kalman filter. It is also notable that the filter was able to correctly approach the inserted bias, with the bias estimation error being close to 0 after the initial convergence. Finally to validate the filter we expose it to real data from the drone, for Experiment E the results are as follows:

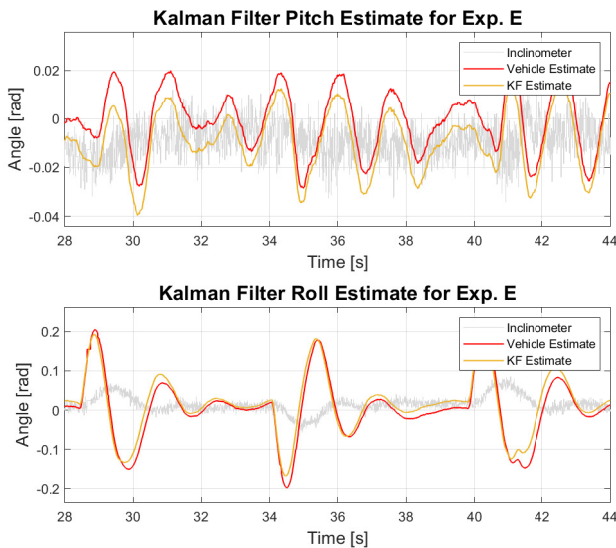


Figure 32: Pitch and roll estimation for Experiment E, compared to vehicle estimate.

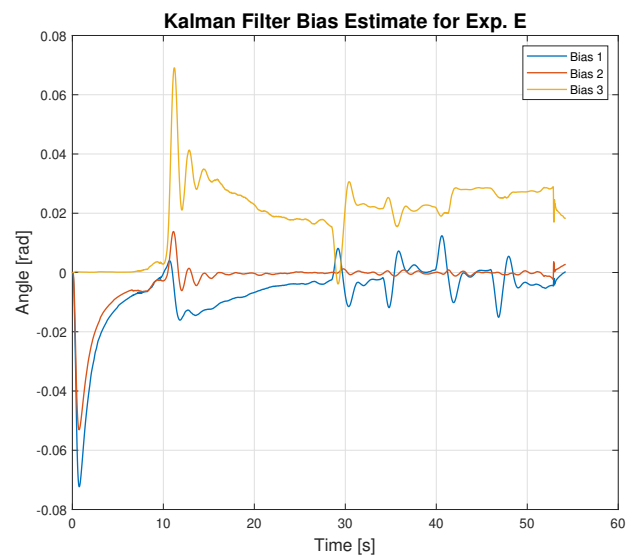


Figure 33: Evolution of the bias for Experiment E.

We can see that the response is close to the one provided by the filter included in the quadrotor. We can also observe that the bias of the terms tends to a non-zero value, which is expected since we know that gyroscopes tend to have bias. Again, a different bias for the accelerometer is probably used by the vehicle estimate since it calibrates before flight and our vehicle contains a damaged support. Although we could tune the parameters of the Kalman filter, it is outside of the scope of this report, we also do not have access to very accurate measurements of the pitch and roll, and our only ground for comparison is another filter. To properly tune the filter, as mentioned before, a MOCAP system could be used to get very accurate attitude measurements and then the filter could be tuned according to those.

References

- [1] Pedro Batista, Carlos Silvestre, and Paulo Oliveira. “Partial attitude and rate gyro bias estimation: observability analysis, filter design, and performance evaluation”. In: *International Journal of Control* 84.5 (2011), pp. 895–903.